Available online at www.sciencedirect.com
ScienceDirect
Journal of Sound and Vibration 303 (2007) 780–797
JOURNAL OF SOUND AND VIBRATION
www.elsevier.com/locate/jsvi

Aspects of computational vibration transmission for sandwich panels

P. Bonfiglio[a], F. Pompoli[a], A.T. Peplow[b,*], A.C. Nilsson[b]

[a]*Department of Engineering, G Saragat 1, University of Ferrara, 44100 Ferrara, Italy*
[b]*Marcus Wallenberg Laboratory for Sound and Vibration Research, Department of Aeronautics & Vehicle Engineering, KTH, S-100 44 Stockholm, Sweden*

Received 24 March 2006; received in revised form 2 February 2007; accepted 5 February 2007
Available online 23 March 2007

Abstract

This paper considers elastic wave propagation and vibration transmission in lightweight composite structures. Specifically a spectral finite element method (SFEM) is developed as an effective numerical tool for the analysis of wave motion in uniform laminated elastic media. In short, SFEM combines a standard finite element method in the direction of layering together with analytical solutions for the remaining direction. This partial discretization leads naturally, via the variational formulation, to dispersion relations for uniform sections of built-up laminates and thus provides valuable information for a wave propagation analysis. Dynamic responses of the vibrating structures are also investigated and numerical simulations compared against a standard finite element method. The predicted transfer accelerances obtained for the steel beam and two sandwich panels are compared with measured data from laboratory experiments.

1. Introduction

Sandwich plates are widely used in many technical applications, as this composition of a thin-walled structure conveniently combines the properties of a high strength. Essentially, there are two possibilities to describe dynamics of sandwich plates. Firstly some hypotheses may be adopted concerning the deformation of an arbitrary cross-section of the layers and reduced equations may be derived [1,2]. The reduced formulations, modified Timoshenko or Euler–Bernoulli theory for example, do not permit the capture of short-wave, high-frequency motions in sandwich plates, but the essential features of wave propagation in these structures have been shown to be valid in an audio-frequency range. Secondly the equations of motion for the "skins" and "core" may be formulated in the framework of a theory of elasticity, which may be solved with continuity conditions at the interfaces between layers, a natural setting for a variational formulation. This is the approach taken here.

In this work the transmission and propagation of vibrations through simple laminated sandwich structures is investigated computationally and experimentally. A number of computational methods, in particular the finite

*Corresponding author. Fax: +46 8 7906122.
E-mail address: atpeplow@kth.se (A.T. Peplow).

0022-460X/$ - see front matter © 2007 Elsevier Ltd. All rights reserved.
doi:10.1016/j.jsv.2007.02.002

element method, are robust techniques that predict dynamic responses with complex geometrical and material structures. However, there are many limitations to numerical predictions. Namely, the simulation of high-frequency excitation for many structures of interest require extremely large computing resources usually beyond a reasonable research budget. Spectral methods are now an established alternative to finite difference and finite element methods to solve elliptic partial differential equations. Techniques such as spectral methods, which capture some dynamics of a problem, are naturally chosen to solve problems in regular rectangular, cylindrical or spherical regions. Specifically the spectral finite element method (SFEM) has been used mainly in the context of structural vibrations; its early history can be found in Ref. [3] and later in the comprehensive review by Williams and Wittrick [4]. In the SFEM, adopted here, the region of interest is decomposed into rectangular elements. Then a variational formulation, of the underlying equations of motion, is approximated with trial functions that are conforming across element boundaries, thus automatically fulfilling coupling conditions in the region. Exploiting the regular Cartesian rectangular domain the physical field of interest may be separated in each element by a combination of polynomials in the transversal z-direction with wave influence functions in the longitudinal x-direction. Subsequently eigenfunctions of a derived differential operator are chosen as wave propagation trial functions in the description of the local *spectral element*. Since the spectral element does not rely on any wavelength-dependent discretization in the longitudinal direction the SFEM can be applied to fairly short as well as very long wave propagation problems. The SFEM has also been applied, in various forms, to a number of acoustic and structural waveguide problems. In particular the method used in Refs. [5,6] can be viewed as a merger of the dynamic stiffness method and the finite element method. The principle of the method is based on a variational formulation for non-conservative motion in the frequency domain. The SFEM has also been used to study vibration in beam frame-works [5], for fluid-filled pipes [6], and recently for acoustic ducts [7]. Use of a variational formulation for the spectral method provides a natural basis for approximations and a straightforward method for combination with standard finite elements.

The use of a one-dimensional finite element scheme to describe the cross-sectional deformation of a laminate has been proposed by Dong and Nelson [8,9], Lundberg et al. [10], Datta et al. [11], Xi et al. [12], and Shorter [13]. Peplow and Finnveden [14] developed the method further to describe ground vibration transmission over a layered bedrock medium with a single object inclusion. Essentially all the previous analyses show how the characteristic equation for free-wave propagation can be formulated as a linear eigenvalue problem in frequency. Datta et al. [11] investigated the dispersion curves of anisotropic laminates and Dong and Nelson [8] assumed the state of plane strain in order to simplify the algebra which was later extended by Shorter [13] for modelling the structural–acoustic response of sandwich panels and constrained layer damping treatments. Xi et al. [12] adopted a finite element based method, similar to the previous approaches for rectangular structures, to investigate the dispersion curves of elastic laminated composite cylinders.

The paper is organized as follows. In Section 2 the variational principle for non-conservative acoustic motion is stated and a description of the trial functions is given and associated dynamic stiffness matrices are presented. Dispersion relations and elastic responses for various plate structures are shown in Section 3 with comparison to measurement data. Some conclusions are given in Section 4.

2. Theoretical models

Consider the cross-section of the sandwich laminate illustrated in Fig. 1(a) and the panels considered in the study illustrated in Fig. 1(b). The laminate consists of an arbitrary number of solid linear viscoelastic and elastic layers and possesses the same properties as a layered waveguide. The current analysis assumes that the layers are planar and isotropic. Uniform properties along the x-direction are assumed in the waveguide formulation described here. For the cross-section in the z-plane, polynomial displacement functions are prescribed, whereas the nodal displacements are here considered functions of x. The displacement functions are used as test functions in a variational approach and the equations of motion for a layered element may be defined.

2.1. Variational form

For the virtual work formulation one may follow standard methods whereby a Lagrangian formulation is devised and minimized for the motion of the system subject to the boundary conditions [15]. Displacements,

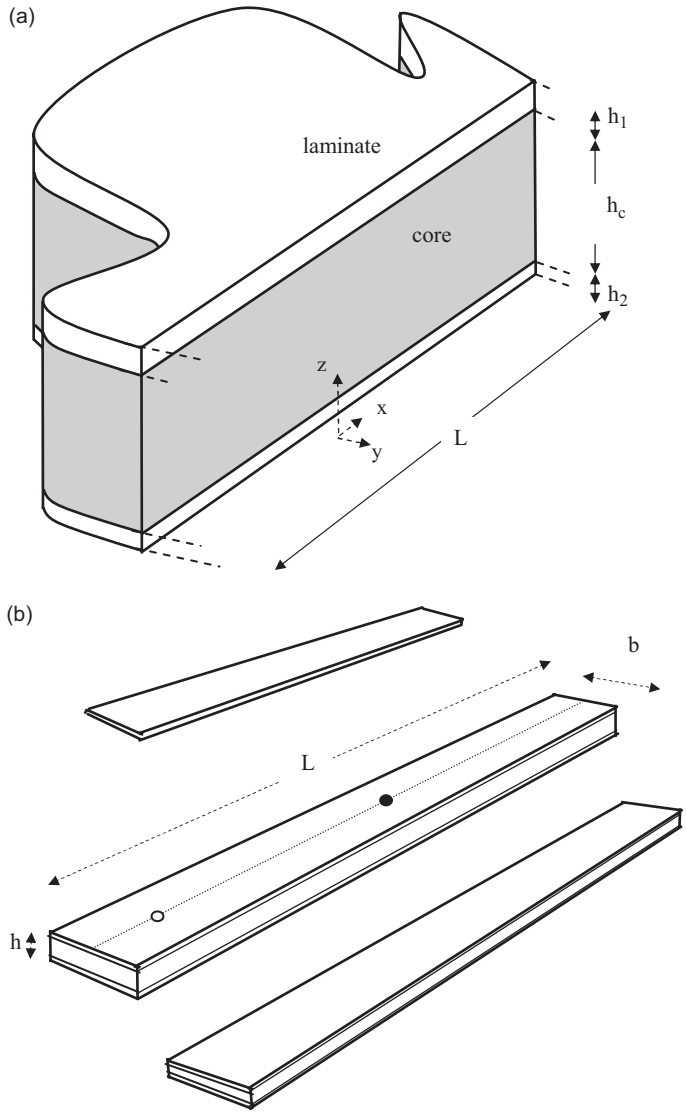

Fig. 1. (a) Configuration of typical sandwich laminate structure in the $x-z$ plane; (b) geometry of each panel from top to bottom: steel panel, total thickness $h = 1.0$ mm, width $b = 0.12$ m, and length $L = 1.0$ m; ceramic panel, total thickness $h = 55$ mm, width $b = 0.15$ m, and length $L = 1.65$ m (showing typical positions of hammer excitation and accelerometer by circle and filled circle along centre line, respectively); aluminium foam panel, total thickness $h = 12$ mm, width $b = 0.12$ m, and length $L = 1.2$ m.

stresses and strains in a particular rectangular region, Fig. 1(a), may be denoted by $\boldsymbol{u}(\boldsymbol{x}, t)$, $\boldsymbol{\sigma}(\boldsymbol{x}, t)$, and $\boldsymbol{\varepsilon}(\boldsymbol{x}, t)$, respectively, and $\boldsymbol{x} = (x, z)$. To represent a wave propagating in the direction of the waveguide, displacements of the form: $\boldsymbol{u}(\boldsymbol{x}, t) = \mathrm{Re}\{\boldsymbol{U}(z)\,\mathrm{e}^{\mathrm{i}(\omega t - \zeta x)}\}$, where $\boldsymbol{U}$ represents a cross-sectional mode shape, ζ the wavenumber constant and ω the angular frequency.

The formulation of the governing equations is based on two-dimensional linear elasticity. The mechanical variables are the displacement $\boldsymbol{u}$, stress $\boldsymbol{\sigma}$, and strain $\boldsymbol{\varepsilon}$ with components

$$\boldsymbol{u} = (u, w)^{\mathrm{T}}, \quad \boldsymbol{\sigma} = (\sigma_{xx}, \sigma_{zz}, \sigma_{xz})^{\mathrm{T}}, \quad \boldsymbol{\varepsilon} = (\varepsilon_{xx}, \varepsilon_{zz}, \varepsilon_{xz})^{\mathrm{T}}. \tag{1}$$

The stress–strain constitutive relations for each sub-region material are given by

$$\boldsymbol{\sigma} = [\mathbf{C}]\boldsymbol{\varepsilon}, \tag{2}$$

where [**C**], the symmetric (3 × 3) matrix, contains the rectilinear elastic moduli. The linear strain-displacement equations are written in split-operator form according to the coordinates (x, z),

$$\boldsymbol{\varepsilon} = \mathbf{L}(\boldsymbol{u}) = \left(\hat{\nabla}_z + \hat{\nabla}\frac{\partial}{\partial x}\right)\boldsymbol{u}, \tag{3}$$

where

$$\hat{\nabla}_z = \begin{bmatrix} 0 & 0 \\ 0 & \dfrac{\partial}{\partial z} \\ \dfrac{\partial}{\partial z} & 0 \end{bmatrix}, \quad \hat{\nabla} = \begin{bmatrix} 1 & 0 \\ 0 & 0 \\ 0 & 1 \end{bmatrix}. \tag{4}$$

The governing equations of motion for the elastic material are derived by Hamilton's principle [15]

$$\delta \int \left(\int_V T - (U + V)\, \mathrm{d}\Omega \right) \mathrm{d}t = 0, \tag{5}$$

where T is the kinetic energy, U the strain energy and V the potential energy due to external forces and δ represents a first variation. The kinetic energy T in terms of the velocity vector $\dot{\boldsymbol{u}}$, and strain energy U in terms of the stress, are given by

$$T = \frac{1}{2}\int \int_\Omega \dot{\boldsymbol{u}}^{\mathrm{T}}[\boldsymbol{\rho}]h\dot{\boldsymbol{u}}\, \mathrm{d}\Omega, \quad U = \frac{1}{2}\int \int_\Omega \boldsymbol{\varepsilon}^{\mathrm{T}}[\mathbf{C}]\boldsymbol{\varepsilon}\, \mathrm{d}\Omega, \tag{6}$$

where $[\boldsymbol{\rho}] = \left[\begin{smallmatrix} \rho & 0 \\ 0 & \rho \end{smallmatrix}\right]$ is the 2 × 2 mass density matrix, h is thickness of structure, and for a plane-strain problem the stiffness matrix, [**C**] is given by

$$[\mathbf{C}] = \frac{Eh}{(1+\nu)(1-2\nu)} \begin{bmatrix} (1-\nu) & \nu & 0 \\ \nu & (1-\nu) & 0 \\ 0 & 0 & \dfrac{1}{2}(1-2\nu) \end{bmatrix},$$

where E denotes (a complex valued) Young's modulus, and ν the Poisson ratio. The potential energy V hereforth consists of applied traction acting on the boundary

$$V = -\int_{\Gamma_j} \dot{\boldsymbol{u}}^{\mathrm{T}}\boldsymbol{\sigma}_n\, \mathrm{d}x, \tag{7}$$

where $\boldsymbol{\sigma}_n$ denotes normal and shear tractions at the boundary. A modified version of Hamilton's principle in the frequency domain will be used here for the dissipative motion, see Ref. [5], since material is modelled through a complex form of Young's modulus, $E = E_0(1 + \mathrm{i}\eta)$ where $\eta > 0$ represents damping as a material loss factor. Performing the variational operation on Eq. (5), and carrying out a partial integration with respect to time, and assuming harmonic time dependence, $\mathrm{e}^{-\mathrm{i}\omega t}$, one obtains

$$\int_\Omega \omega^2(\delta\boldsymbol{u}^a)^{\mathrm{T}}h[\boldsymbol{\rho}]\boldsymbol{u} - \mathbf{L}(\delta\boldsymbol{u}^a)^{\mathrm{T}}[\mathbf{C}]\mathbf{L}(\boldsymbol{u})\, \mathrm{d}\Omega = \mathbf{0}, \tag{8}$$

where superscript ^{a} denotes complex conjugate in the adjoint system having negative damping and virtual quantities are denoted by δ.

It is understood that the stiffness matrix [**C**] takes a complex form in the following analysis and calculations. In Eq. (8), only the adjoint of the displacement functions and their derivatives are being varied. During the variational process, the longitudinal and vertical displacements u and w and their derivatives are viewed as being independent from their complex conjugates. The underlying differential equation is linear and hence this approach is in effect equivalent to varying the real and imaginary parts of the functions independently.

2.2. Numerical modelling

In elastic waveguides with constant geometrical cross-section, the solutions of the governing equations of motion are a combination of exponential terms describing the propagation with cross-sectional modes. Thus, the axial x-dependence is separable from the cross-sectional z-dependencies. In this case, the application of the finite element method, the displacement field of the cross-section of a rectangular element may be represented by high-order polynomials, $N_j(z), j = 1, \ldots, M$, Ref. [7]. For in-plane motion a combination of polynomials is assumed. In the finite element discretization a cross-section is divided so that material parameters are constant within each interval. Within one *spectral finite element*, the in-plane displacement field may be represented in the coordinate system such that a dimensionless $2 \times 2m$ real-valued matrix $[\mathbf{N}(z)]$ with the given coordinate functions as elements, and a $2m \times 1$ vector $\hat{\mathbf{u}}(x)$ has the dimension of length,

$$\mathbf{u}(x, z) = [\mathbf{N}(z)]\hat{\mathbf{u}}(x), \tag{9}$$

where the displacement function, $\mathbf{u}(x, z) = [u(x, z), w(x, z)]^{\mathrm{T}}$,

$$u(x, z) = [N_1(z), 0, N_2(z), \ldots, 0, N_M(z), 0]\hat{\mathbf{u}}(x),$$
$$w(x, z) = [0, N_1(z), 0, \ldots, N_{M-1}(z), 0, N_M(z)]\hat{\mathbf{u}}(x)$$

using M piecewise polynomial shape functions, compactly supported over each interval in the vertical direction. Elemental shape functions $\hat{\mathbf{u}}(x)$ will be defined later in the article.

Partial integration in the x-direction, assuming $\Omega = H \times T$, where $T \coloneqq \{x : -D \leqslant x \leqslant +D\}$, and H denotes the uniform cross-section interval, leads to an expression given in Appendix, Eq. (18). The final integral expression in Eq. (18) provides boundary conditions at the cross-section extremities. It is clear that this is the *natural boundary condition* describing a stress-free condition. Since $\delta\hat{\mathbf{u}}$ is arbitrary and $\hat{\mathbf{u}}$ is a function of the axial direction only, Eq. (18) yields a system of second-order differential equations. Hence the formulation involves evaluating the derivatives and the integrals over z, and then integration by parts for the x-dependence. Written as an analogy of Eq. (8), assuming a stress-free boundary:

$$\int (\delta\mathbf{u}^a)^{\mathrm{T}} \left([\mathbf{K}_2]\frac{\mathrm{d}^2}{\mathrm{d}x^2} + [\mathbf{K}_1]\frac{\mathrm{d}}{\mathrm{d}x} + [\mathbf{K}_0] - \omega^2[\mathbf{M}] \right) \hat{\mathbf{u}}\, \mathrm{d}x = 0. \tag{10}$$

The system of equations, derived from Eq. (10), possesses constant matrix coefficients in the form of square $(m \times m)$ matrices $[\mathbf{K}_2]$, $[\mathbf{K}_1]$, $[\mathbf{K}_0]$, and $[\mathbf{M}]$. Hence, the solutions of the linear homogeneous system, $\hat{\mathbf{u}}_l = (U_l(x), W_l(x))^{\mathrm{T}}$, may be written as:

$$U_l(x) = c_l \mathbf{\Phi}_l \, \mathrm{e}^{\mathrm{i}\zeta_l x}, \quad l = 1, \ldots, m,$$
$$W_l(x) = d_l \mathbf{\Phi}_{m+l} \, \mathrm{e}^{\mathrm{i}\zeta_{m+l} x}, \quad l = 1, \ldots, m, \tag{11}$$

where $\mathbf{\Phi}_l$ is a vector representing the nodal amplitudes $(\Phi_{1,l}, \Phi_{m,l})$, $(\Phi_{1+m,l}, \Phi_{2m,l})$, and interior amplitudes $(\Phi_{j,m}, 2 \leqslant j \leqslant m-1)$, $(\Phi_{j+m,m}, 2 \leqslant j \leqslant 2m-1)$ and c_l, d_l are arbitrary constants. Under this assumption a nonlinear eigenvalue problem arises, $\mathbf{K}(\zeta)\mathbf{\Phi} = \mathbf{0}$, which may be cast, simply, as a polynomial eigenvalue problem,

$$[\mathbf{K}(\zeta)]\mathbf{\Phi} = \{\zeta^2[\mathbf{K}_2] - \mathrm{i}\zeta[\mathbf{K}_1] - [\mathbf{K}_0] + \omega^2[\mathbf{M}]\}\mathbf{\Phi} = \mathbf{0} \tag{12}$$

of order m for the variable ζ.

The eigenvalue problem relates the wavenumber ζ to the angular frequency ω, one of them being given and the other being the eigenvalue to be sought. If $\zeta \in \mathbb{R}$ is given, Eq. (12) is a generalized eigenvalue problem with $2m$ eigenvalues ω^2. If instead the angular frequency is given, Eq. (12) is a quadratic eigenvalue problem (QEP) with $4m$ eigenvalues ζ, see Ref. [16] for discussion and review of numerical evaluation of QEP. In the latter case, the eigenvalues are generally complex-valued and correspond to evanescent waves. For real values of the wavenumber eigenvalues, ζ, corresponding to propagating waves, it is possible to find associated dispersion relations for the layered system and is discussed further in Section 3.2.

The eigenvalue problem may be reduced to first-order form by introducing an auxiliary parameter, $\gamma = \mathrm{i}\zeta$ and variable $\hat{\mathbf{v}} = \gamma\hat{\mathbf{u}}$. With this change of variables the polynomial eigenvalue problem (12) may be recast as

a generalized ($4m \times 4m$) linear eigenvalue problem known as a *second companion* form in Ref. [16],

$$[\mathbf{A}]\hat{\mathbf{V}} = \gamma[\mathbf{B}]\hat{\mathbf{V}}, \tag{13}$$

where

$$[\mathbf{A}] = \begin{bmatrix} -\mathbf{K}_0 + \omega^2\mathbf{M} & \mathbf{0} \\ \mathbf{0} & \mathbf{I}_{2m} \end{bmatrix}, \quad [\mathbf{B}] = \begin{bmatrix} \mathbf{K}_1 & \mathbf{K}_2 \\ \mathbf{I}_{2m} & \mathbf{0} \end{bmatrix}, \quad \hat{\mathbf{V}} = \begin{bmatrix} \hat{\mathbf{u}} \\ \gamma\hat{\mathbf{u}} \end{bmatrix}.$$

The resolution of the matrix eigenvalue problem, Eq. (13) is itself easily achieved by a number of standard computational routines where *damping* is included in the model, i.e. the value of the loss factor η is positive. In the present analysis a *QZ* algorithm with Cholesky factorization was used. This produces a set of eigenvalues γ_l, $l = 1, \ldots, 4m$ and corresponding cross-sectional mode shapes or waveforms. Note that for zero damping $\eta = 0$ the polynomial eigenvalue problem is of Hamiltonian type and care must be taken in evaluating the eigenvalues as discussed in Ref. [16]. It has been found that some eigenvalues, γ, violate the complex conjugate pairing rule especially when located close to the imaginary axis. This lead to instability issues for zero and also for very small values of damping $\eta \approx 0.1\%$. This may be overcome using other methods such as Van Loan's square-reduced algorithm [17] but is yet to be resolved.

Final construction of the set of basis functions, Eq. (9) and local dynamic stiffness matrix, defined over the region $\Omega_j \coloneqq H \times T$, where $T \coloneqq \{x : -D \leqslant x \leqslant +D\}$, is standard and will only be briefly described here. By consideration of the solutions in Eq. (11) it is clear that each wave influence function may be written as a linear combination of these solutions

$$\hat{u}^e_{jk}(x) = \sum_{l=1}^{2m} \Phi_{jl}\mathrm{E}_{ll}(x)X_{lk}\hat{u}_k, \quad j = 1, \ldots, 2m, \;\; k = 1, \ldots, 4m, \tag{14}$$

where entries Φ_{jl} and E_{ll} take the values of eigenvectors and exponential functions, respectively. Coefficients X_{lk} are to be determined by scaling the set of wave influence functions to unity. Substitution of Eq. (9) into Eq. (8), over the local region Ω_j, and using the same matrices as in Eqs. (19)–(22), yields a system of $4m \times 4m$ linear equations. It is necessary to partition the matrix ($2m \times 4m$) of eigenvectors into equal ($m \times 4m$) *longitudinal* and *vertical* partitions such that

$$\mathbf{\Phi} = \begin{bmatrix} \mathbf{\Phi}_u \\ \mathbf{\Phi}_w \end{bmatrix}.$$

Hence the local dynamic stiffness matrix for a certain element may be written as

$$L_{\Omega_j} = \hat{\mathbf{u}}^{a\mathrm{T}}[\mathbf{L}]_{\mathrm{loc}}\hat{\mathbf{u}}, \tag{15}$$

where

$$[\mathbf{L}]_{\mathrm{loc}} = [\mathbf{X}]^{\mathrm{T}}([\mathbf{L}]_{uu} + [\mathbf{L}]_{uw} + [\mathbf{L}]_{wu} + [\mathbf{L}]_{ww}) .* [\mathbf{E}_I][\mathbf{X}], \tag{16}$$

where $.*$ denotes the Schur product and

$$\begin{aligned}
[\mathbf{L}]_{uu} &= -\langle\mathbf{Y}\rangle\mathbf{\Phi}_u^{\mathrm{T}}[\mathbf{K}^2_{uu}]\mathbf{\Phi}_u\langle\mathbf{Y}\rangle + \mathbf{\Phi}_u^{\mathrm{T}}([\mathbf{K}^0_{uu}] - \omega^2[\mathbf{M}_{uu}])\mathbf{\Phi}_u,\\
[\mathbf{L}]_{uw} &= -\langle\mathbf{Y}\rangle\mathbf{\Phi}_u^{\mathrm{T}}[\mathbf{K}^1_{uu}]\mathbf{\Phi}_w + \mathbf{\Phi}_u^{\mathrm{T}}[\mathbf{K}^1_{uw}]\mathbf{\Phi}_w\langle\mathbf{Y}\rangle,\\
[\mathbf{L}]_{wu} &= -\langle\mathbf{Y}\rangle\mathbf{\Phi}_w^{\mathrm{T}}[\mathbf{K}^1_{wu}]\mathbf{\Phi}_u + \mathbf{\Phi}_w^{\mathrm{T}}[\mathbf{K}^1_{ww}]\mathbf{\Phi}_u\langle\mathbf{Y}\rangle,\\
[\mathbf{L}]_{ww} &= -\langle\mathbf{Y}\rangle\mathbf{\Phi}_w^{\mathrm{T}}[\mathbf{K}^2_{ww}]\mathbf{\Phi}_w\langle\mathbf{Y}\rangle + \mathbf{\Phi}_w^{\mathrm{T}}([\mathbf{K}^0_{ww}] - \omega^2[\mathbf{M}_{ww}])\mathbf{\Phi}_w,
\end{aligned}$$

where $\langle\mathbf{Y}\rangle$ represents a diagonal matrix created from the vector of calculated wavenumbers, ζ_i, from eigenvalue problem (12). Within the computations of local dynamic stiffness matrices defined over a beam span, $-D \leqslant x \leqslant +D$, use is made of the matrix generating function over the width of the element

$$[\mathbf{E}_I(\mathbf{Y}, D)] = \int_{-D}^{D} \exp(\mathbf{Y}x - \mathbf{Y}^p D)\exp(\mathbf{Y}x - \mathbf{Y}^p D)^{\mathrm{T}}\,\mathrm{d}x, \tag{17}$$

which has an analytic form detailed in Ref. [6]. The convention that the exp function preserves the dimension of column vectors has been adopted. Generating the $\mathbf{E}_I$ matrix was performed only once thus decreasing overall dynamic stiffness matrix computation substantially. For problems with *short* waveguides, (small D) or *small* valued entries in $\{\mathbf{Y}\}$ a Taylor expansion series for each integrated expression was performed.

Evaluation of the dynamic stiffness matrix above applies to a single spectral finite element. The matrix is full, complex and symmetric. For a combination of finite elements, describing a general elastic domain, the corresponding dynamic stiffness matrix has a block diagonal structure; each block derived from the expression in Eq. (16). The description above and in the previous section applies to a layered waveguide where a cross-section is discretized by locating appropriate interface nodes. Wave functions are subsequently found for the composed layers, by imposing displacement continuity at the interface, thus increasing the size of the matrix eigenvalue problem. Construction of stiffness matrices follows as with construction of stiffness matrices for a single layer waveguide. Hence it is possible to solve multi-layered sandwich panel problems using super-spectral elements bearing in mind the large generalized matrix eigenvalue problems to be solved.

A force may be easily included into the model if defined at a finite element nodal point. The complete element formulation, for an arbitrary element length, element, including assembling element matrices, solving a dispersion relation, evaluating the dynamic stiffness matrix and solving a typical problem, as in Section 3.3, requires only 0.351 CPU seconds, per frequency step, on a 1.3 GHz PC for a 66 degree-of-freedom linear system.

3. Results

The efficiency and accuracy of the spectral finite element scheme for three sample panels will now be presented. Note that longitudinal motion of the panels has not been considered in this section. This is principally due to well-known difficulties in their measurement but also the objective in this work has been in vertical vibrations; the main mechanism behind structure-borne sound. First a description of the measurements taken is given.

3.1. Measurements

Three different structures were tested in the present work: a steel beam, a lightweight aluminium sandwich panel and a non-symmetric ceramic panel. The physical parameters of the samples used are listed in Table 1. The experimental procedure used in this work was simply based on the measurement of frequency response of an accelerometer mounted on the tested panel excited by an impact hammer and is sketched in Fig. 2. The set-up consisted of an accelerometer Bruel & Keir (B&K) type 4393 (2.4 g), a B&K type 8202 impulse hammer, two charge amplifiers B&K type 2635, and a two channel signal analyser HP 3562A. The samples were suspended, by means of rubber strings, with both ends free. In order to obtain values for the mechanical parameters of the homogeneous steel beam (i.e. Young modulus) and the sandwich structures components (i.e. Young modulus of the laminates and shear modulus of the core), measurements on the panels with

Table 1
Material constants and dimensions for panels shown in Fig. 1(b)

Material property	Steel panel	Ceramic panel laminate	Ceramic panel core	Aluminium panel laminate	Aluminium panel core
Density, ρ (kg/m^3)	7850	1580	101	2250	142
Young's modulus (N/m^2)	2.05×10^{11}	8.70×10^{9}	1.40×10^{8}	5.70×10^{10}	2.80×10^{8}
Shear modulus (N/m^2)	7.80×10^{10}	3.34×10^{9}	5.37×10^{7}	1.78×10^{10}	1.09×10^{8}
Poisson ratio	0.3	0.3	0.3	0.3	0.3
Loss factor	0.0015	0.001	0.04	0.001	0.01
Thickness (h_1, h_2) (mm)	—	2.5/2.5	—	1.0/1.0	—
Core thickness (h_c) (mm)	1.0	—	50.0	—	10.0
Length (m)	1.0	1.65	—	1.20	—

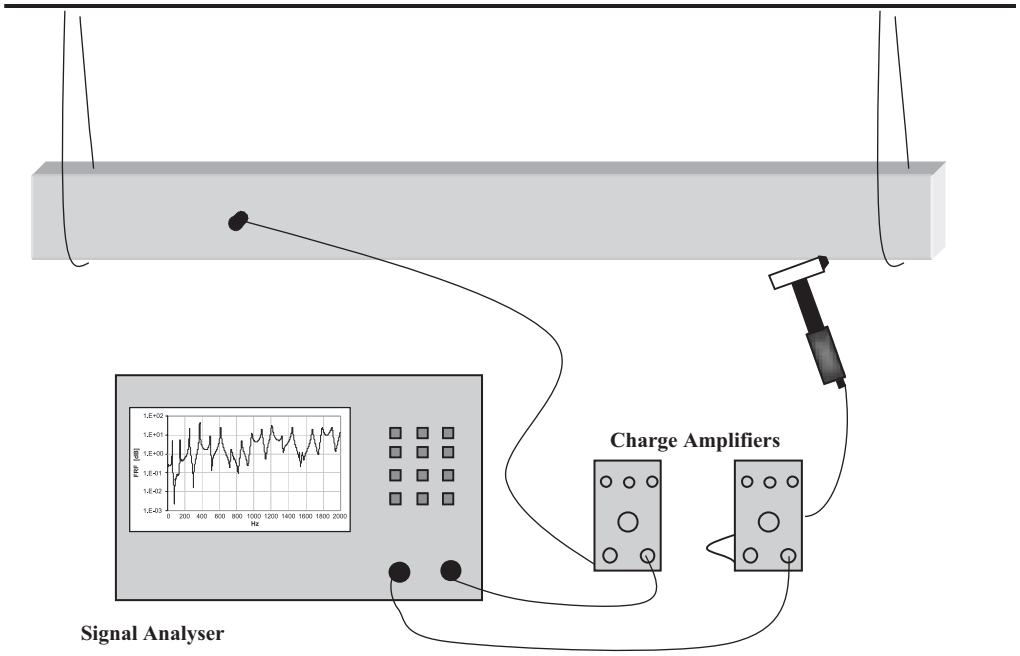

Fig. 2. Experimental setup.

accelerometer and impact source were as close to the ends as possible were carried out. For the steel beam Bernoulli–Euler beam theory, giving the bending stiffness as functions of the eigenfrequencies, was employed. It has to be remarked that due to difficulties in suspending the panels, measurements were carried out from 5.0 to 500.0 Hz for the steel beam (2500.0 for sandwich panels) with a frequency resolution selected of 2.5 Hz. In addition an exponential window was applied to the captured signals.

Sources of possible errors in the measurements could have been low noise-to-signal ratio due to low excitation force impulse or on the other hand nonlinear response caused by too high impulse force. A coherence function was recorded during the measurements indicated the frequency range where poor quality responses were present and are shown later in the results section. Other possible sources of error include the mass effect of the attached accelerometer, and the potential presence of cross modes in the high-frequency range. It was found that the accelerometer mass had only a small influence at resonance frequencies. The first cross-modes generated for the studied panels corresponded to frequencies above 2.5 kHz in all three cases.

For the sandwich structures an inverse strategy for the estimation of material properties was used, based on sixth-order theory, see Ref. [1]. This method makes use of sixth-order Timoshenko theory, giving an accurate estimation of the eigenfrequencies and the flexural response of sandwich panels. The method minimizes the model eigenfrequencies against the measured eigenfrequencies in a least squares sense with respect to the input variables, i.e. the elasticity modulus of the laminates and the shear modulus of the core. Accuracy up to two significant digits was chosen.

3.2. Dispersion relations

The eigenvalues, ζ, also referred as wavenumbers, are solved numerically for a given frequency once the equations of motion have been assembled through solutions of the QEP Eq. (12).

In Fig. 3 the case of a simply free–free steel plate is investigated. The resulting dispersion curves using five element layers are shown, where the material characteristics and geometry of the plate are given in Table 1. Five quadratic polynomial functions, see Eq. (9) were used to describe the displacement yielding a 22×22 QED. No internal damping term was included here and the known analytical wavenumbers for flexural waves for thin isotropic plate, given by $k_1 = (12(1-\nu^2)\rho/E_0h^2)^{1/4}\omega^{1/2}$, $k_2 = (2(1+\nu)\rho/E_0)^{1/4}\omega^{1/2}$, [18] with

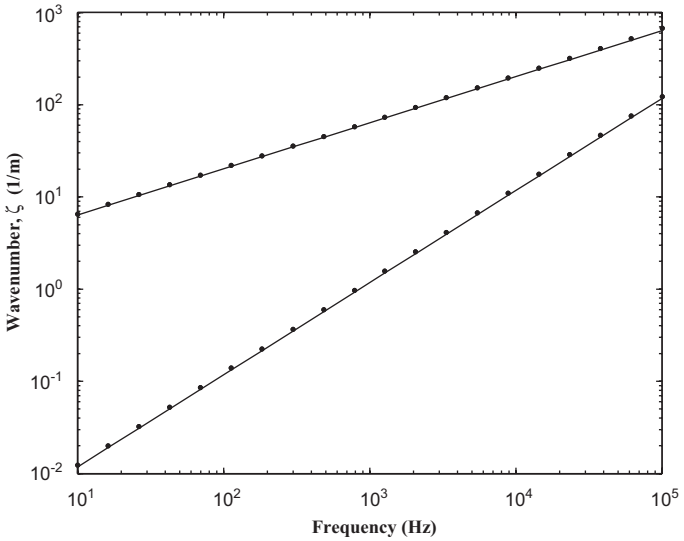

Fig. 3. Propagating wavetypes for a 1.0 mm thick steel panel: solid line, analytical results: dots, SFEM computed results.

thickness h are shown for comparison. The analytical and predicted dispersion curves are in good agreement and with more elements or increasing polynomial order the relative error of the predicted wavenumbers decreases, see Ref. [7] for an analogous acoustic problem.

The spectral dispersion relation approach was used to calculate the wave types for typical elastic sandwich panels. Most sandwich panel cores are orthotropic; however, for our analysis the following examples assume an isotropic core. The effective isotropic properties of an *aluminium foam* core with steel laminates was used in the first sandwich example and are given by: $E_0 = 280 \times 10^6\,\mathrm{N/m^2}$, $\nu = 0.3$, $\rho = 142\,\mathrm{kg/m^3}$. The skins are taken to be aluminium with isotropic properties given by: $E_0 = 57 \times 10^9\,\mathrm{N/m^2}$, $\nu = 0.3$, $\rho = 2250\,\mathrm{kg/m^3}$. A symmetric sandwich construction is considered with 1.0 mm thick skins and a 10 mm thick core. The dispersion curves of the propagating wave types of the sandwich panel were calculated using the spectral element approach and are plotted in Fig. 4. Below approximately 15.0 kHz, two propagating waves exist corresponding to flexural and shear waves. Around 15.0 and 25.0 kHz two additional propagating waves cut-on the higher frequency wave has a negative group velocity and only exists over a very narrow frequency range; the other wave has a positive group velocity and exists over a much broader frequency range.

The effective isotropic properties of a soft foam core with ceramic laminates was used in the second sandwich example and are given by: $E_0 = 140 \times 10^6\,\mathrm{N/m^2}$, $\nu = 0.3$, $\rho = 101\,\mathrm{kg/m^3}$. The skins are taken to be aluminium with isotropic properties given by: $E_0 = 8700 \times 10^6\,\mathrm{N/m^2}$, $\nu = 0.3$, $\rho = 1580\,\mathrm{kg/m^3}$. A symmetric sandwich construction is considered with 2.5 mm thick skins and a 50 mm thick core. The dispersion curves of the propagating wave types of the sandwich panel were calculated using the spectral element approach and are plotted in Fig. 5. Below approximately 4.0 kHz, two propagating waves exist corresponding to flexural and shear waves. Around 4.0 and 6.0 kHz two additional propagating waves cut-on which involve an out-of-phase motion of the skins of the panel in the in-plane direction. At higher frequencies it is evident that additional waves cut-on.

It is well known that Timoshenko theory is not capable of correctly describing sandwich beam vibration as the deformation of the laminates of the sandwich is coupled to the shear deformation of the core. This coupling becomes important in the high-frequency range and effectively stiffens the beam as compared to a homogeneous beam with identical shear modulus and bending stiffness; in principle, the laminates limit the shear deformation of the beam core. Thus, it can be concluded that there are three major mechanisms of deformation governing the vibration of a typical sandwich panel; namely that of pure bending of the entire cross-section, which is a low frequency phenomenon taken into account by classical beam theory; pure shear of the sandwich panel core which dominates the mid-frequency range; and finally that of the bending of the laminates due to shear deformation of the core. Naturally, at yet higher frequencies additional mechanisms

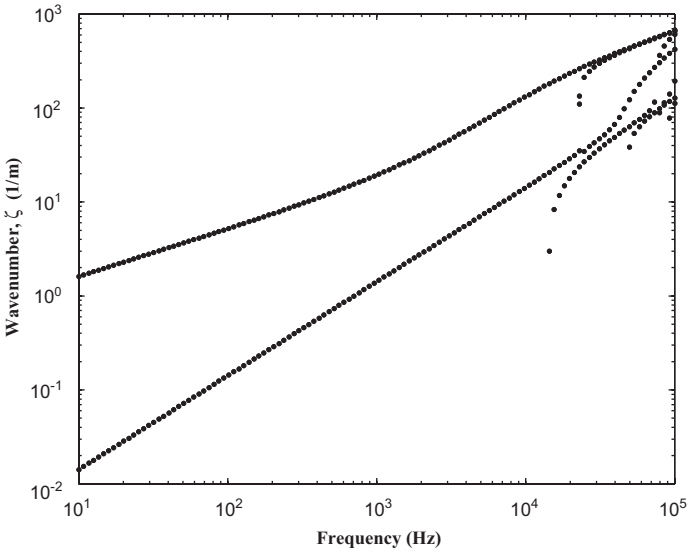

Fig. 4. Propagating wavetypes for a 10.0 mm thick aluminium sandwich panel: dots, SFEM computed results.

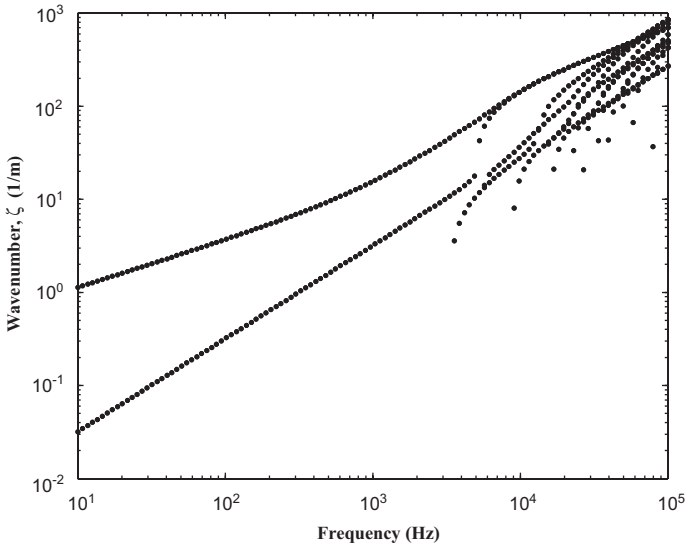

Fig. 5. Propagating wavetypes for a 50.0 mm thick ceramic sandwich panel: dots, SFEM computed results.

become important; however, for typical sandwich panel structures subject to vibration in the audible frequency range ($\leqslant$1.5 kHz) these may often be neglected. In the following section we consider forced responses at frequency ranges well below the cut-on frequency of shear deformations.

3.3. Forced response

To provide a comparison with the numerical results here comparisons were made, in addition with the measurements, with FEMLAB 3.1 results [19]. The geometric properties and the total mass density of the structure are assumed to be known. For the SFEM and standard finite element method the aluminium foam sandwich sample was modelled using a total of 66 degrees of freedom and 14 978 degrees of freedom, respectively. The standard finite element method used cubic polynomials over a triangulated domain; the mesh

of 1593 elements is shown in Fig. 6. Computing time for FEMLAB 3.1 calculations, in direct response computations, totalled around five times that for the SFEM. Total CPU time for the spectral finite element was of the order of just under 5 min on a Pentium IV, 512 Mb 1.3 GHz desktop PC and 20 min using FEMLAB 3.1 software.

Finally measurements for different positions of accelerometers and hammer were carried out. The signals from the impulse hammer force gauge and the accelerometers were conditioned by Bruel & Keir type 2635 charge amplifiers before being sent to a digital spectrum analyser. For each measurement, 10 signals were acquired and the average response determined. The ordinary coherence function was checked to ensure that the data were of acceptable quality. The frequency range of the measurements was 5–500 Hz for the simple steel beam and 5–1.5 kHz for the two sandwich panels with a resolution of 2.5 Hz for each. The lower frequency limit was determined by the low accelerometer sensitivity. At 1.5 kHz, the flexural wavelength would be at least 10 times the depth of the panel so there was no risk of the motion tending toward that of a Timoshenko beam [18].

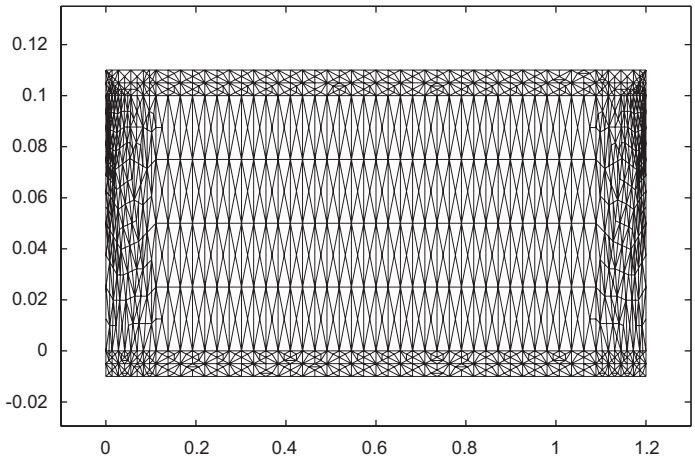

Fig. 6. Finite element mesh (not to scale), FEMLAB [19], using 1593 cubic triangular elements totalling 14 978 degrees of freedom for each frequency. Note the inhomogeneous mesh design featured in the software package.

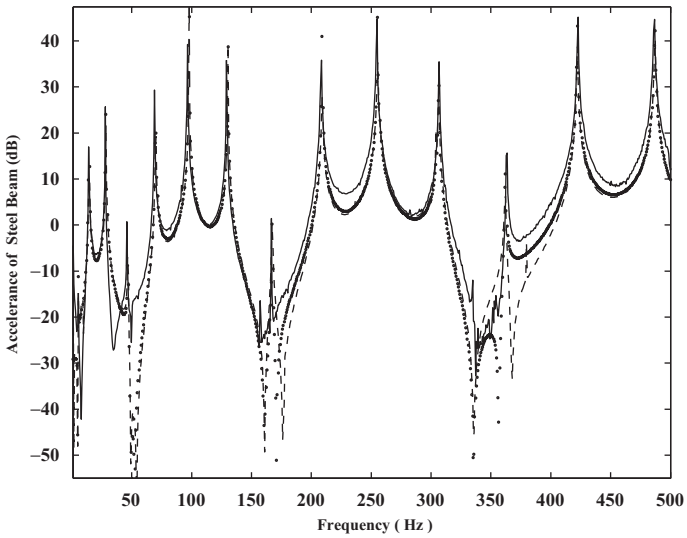

Fig. 7. Acceleration levels at 0.27 m and hammer at 0.74 m from edge. Solid line (-) measurements; dashed line SFEM (–); dots FEMLAB (·) for steel beam.

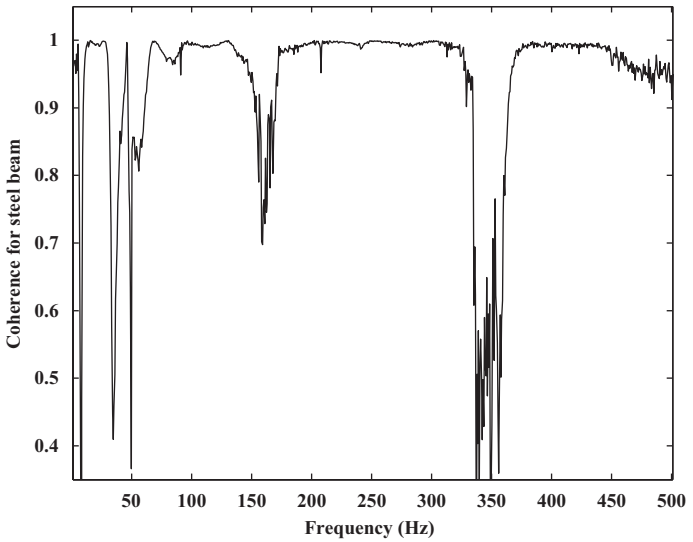

Fig. 8. Coherence at 0.27 m and hammer at 0.74 m from edge for steel beam.

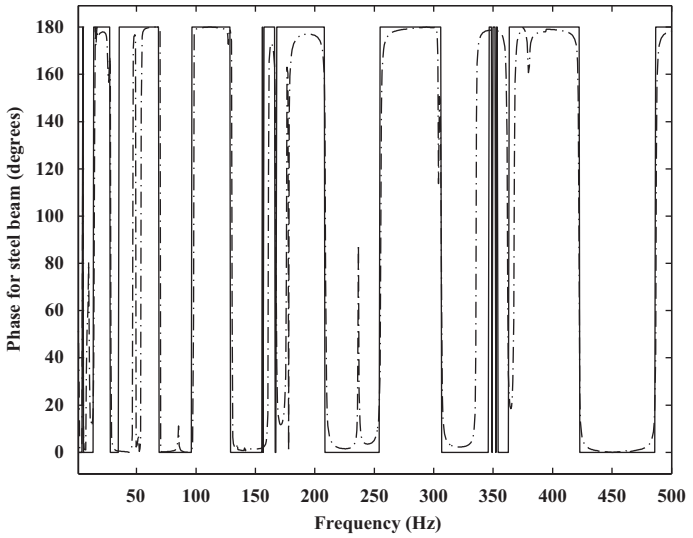

Fig. 9. Phase at 0.27 m and hammer at 0.74 m from edge for steel beam. Solid line (-) measurements; dashed-dot line SFEM (-·) for steel beam.

Comparison for amplitude of the acceleration between experimental results, SFEM and FEMLAB [19] and phase between SFEM and measurements are reported in Figs. 7–15.

3.3.1. *Steel beam*

Fig. 7 compares the predicted transfer accelerance for the steel beam structure from Table 1, using a standard finite element scheme and the spectral element method and the measured response. The following observations are made:

(a) Both numerical methods agree with the measured response for the homogeneous steel beam in the frequency range given; almost indistinguishable transfer accelerance in Fig. 7 except at anti-resonances. Differences are shown in the coherence Fig. 8 over an extended frequency range.

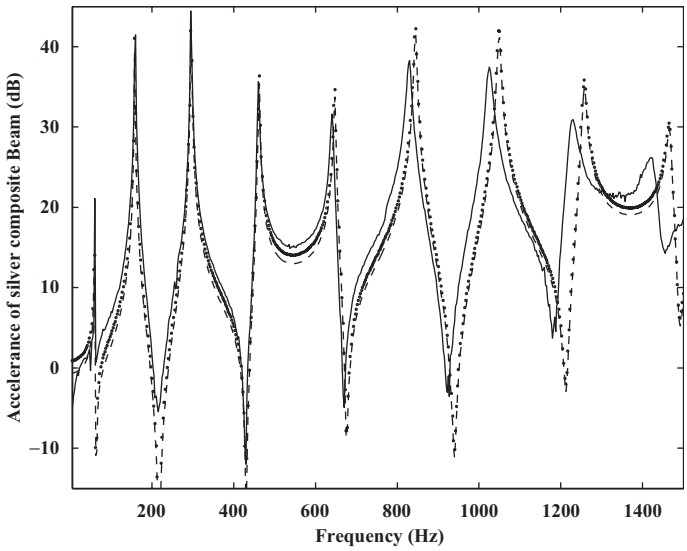

Fig. 10. Acceleration levels at 1.2 m and hammer at 0.9 m from edge. Solid line (-) measurements; dashed line SFEM (–); dots FEMLAB (·) for aluminium foam sandwich panel.

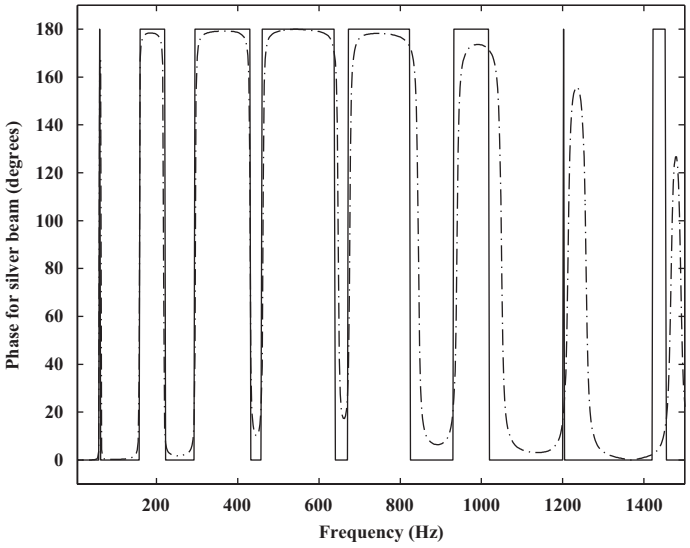

Fig. 11. Phase at 1.2 m and hammer at 0.9 m from edge. Solid line (-) measurements; dashed-dot line SFEM (-·) for aluminium foam sandwich panel.

(b) The transfer accelerance is over-predicted by the numerical models except in narrow band resonant regions. This may be due to small mass sensitivity effecting vibrations in these regions, evident in the phase, Fig. 9.

Over the frequency range, the average relative error between the FEMLAB 3.1 and SFEM numerical methods and the measured data were 2.5% and 2.6% respectively.

3.3.2. *Aluminium foam sandwich panel*

Fig. 10 compares the predicted transfer accelerance and phase for the aluminium foam sandwich structure from Table 1, using a standard finite element scheme and the spectral element method and the measured

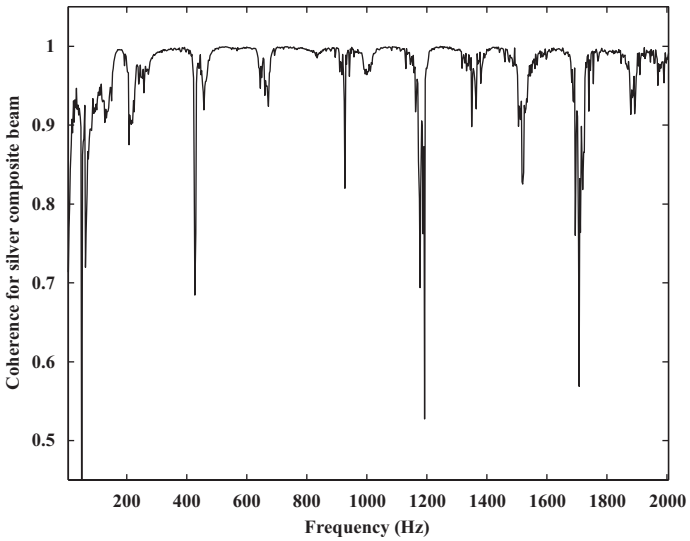

Fig. 12. Coherence at 1.2 m and hammer at 0.9 m from edge for aluminium foam sandwich panel.

response and Fig. 11 compares the phase. The following observations for the aluminium foam sandwich sample were made.

(a) The numerical methods agree with the measured resonance data in the total frequency range up to 600 Hz but above which each method overpredicts the resonant frequencies against the measured data.
(b) The standard finite element method overpredicts the accelerance below 600 Hz whereas the spectral finite element underpredicts, the phase behaviour is shown in Fig. 11.
(c) Average relative errors of 2.3% for FEMLAB and 2.4% and SFEM were obtained. Coherence for the measurements is shown in Fig. 12 shows good coherence up to 2 kHz, opposed to the ceramic panel described next.

The next example shows the limits of comparison for a *thicker* sandwich sample.

3.3.3. Ceramic sandwich panel

Fig. 13 compares the predicted transfer accelerance and phase for the ceramic sandwich structure from Table 1, using a standard finite element scheme the spectral element method and the measured response and Fig. 13 compares the phase. Generally the response is different to the two previous examples, the core is much thicker and lighter than the aluminium foam panel and the following observations were made for the given source and receiver position.

(a) The two numerical methods agree in the frequency range up to 1500 Hz but discrepancies with the measured data appear as low as 800 Hz. The difference is evident in the phase behaviour in Fig. 14 and the coherence, Fig. 15. Note the error of the order of 14 dB at around 1050 Hz, which may be accounted for by the apparent cut-on of shear waves, see Fig. 5, where the laminates are moving out of phase with each other and hence are difficult to record since this motion using the accelerometers and impulse hammer.
(b) Both numerical methods slightly overpredict the transfer accelerance below 600 Hz. Above this frequency the numerical methods significantly underpredict the accelerance. In Fig. 14 the phase shows curious behaviour between 400 and 800 Hz, not observed in the measured data.
(c) Resonant peaks are over-predicted by the numerical methods above 800 Hz, clearly seen in Fig. 13. This is possibly due to the difficulty in estimating the material parameters for the sandwich core, which may not display elastic behaviour. For the ceramic sandwich panel average relative errors of 3.1% for FEMLAB

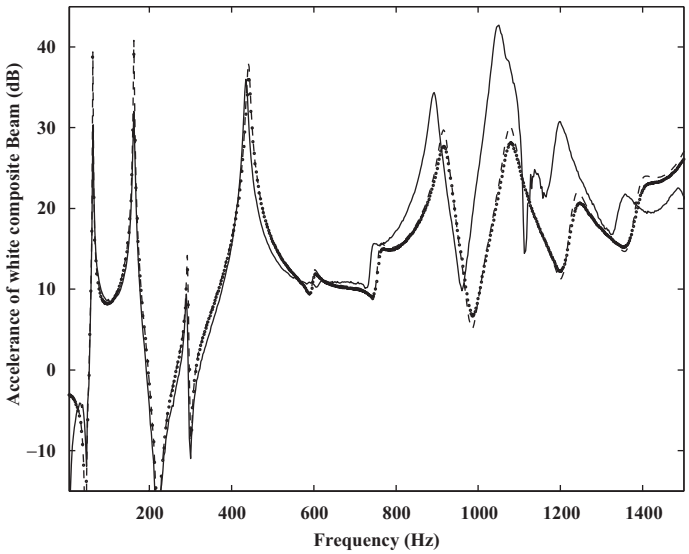

Fig. 13. Acceleration levels at 1.07 m and hammer at 0.68 m from edge. Solid line (-) measurements; dashed line SFEM (–); dots FEMLAB (·) for the ceramic sandwich panel.

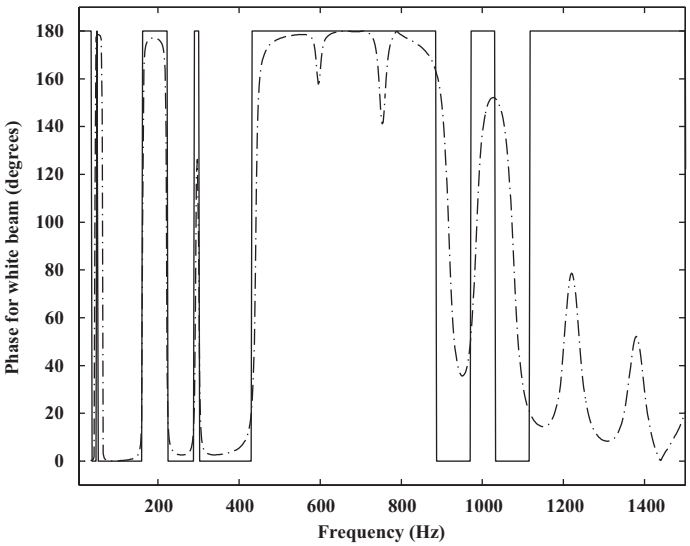

Fig. 14. Phase at 1.07 m and hammer at 0.68 m from edge. Solid line (-) measurements; dashed-dot line SFEM (-·) for the ceramic sandwich panel.

scheme and 3.0% for the SFEM technique. Similar orders of error were also recorded at other receiver points.

4. Conclusion

A spectral finite element developed for the analysis of structural vibration at high frequencies for sandwich panels has been presented. It describes the motion as a combination of travelling and decaying waves along the structure using a low number of degrees of freedom. It has been shown that the SFEM agrees well with

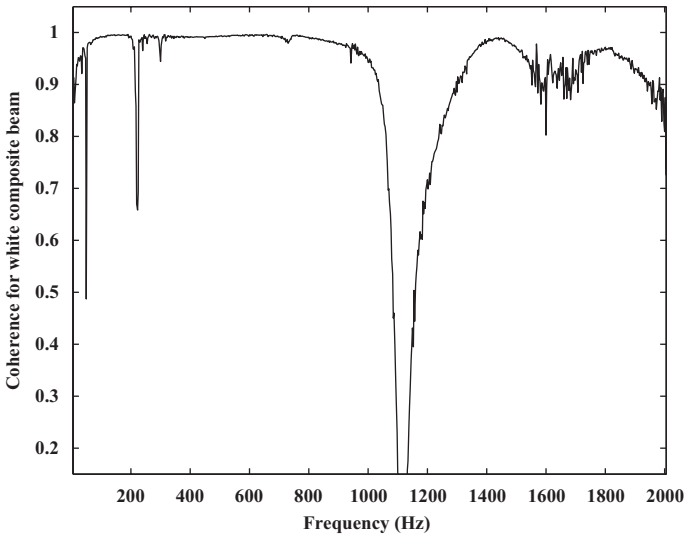

Fig. 15. Coherence at 1.07 m and hammer at 0.68 m from edge for the ceramic sandwich panel.

numerical software. In addition the spectral method has an added bonus of evaluating dispersion relations for "no extra charge". Indeed, it may be possible to use the method in an inverse procedure for defining characteristic parameters for the structure.

The developed laminate model is useful for structures that are uniform along a single coordinate axis but otherwise arbitrary in material composition and geometry. Furthermore, since the cross-section displacement functions are formulated in terms of the nodal displacements using high-order polynomials it can easily be coupled to a conventional finite element method.

(1) With a large cost-saving in computation time over conventional finite elements this numerical method has been shown to have promise for numerical predictions of vibration response for thin and thick laminate structures. For similar orders of magnitude of relative error, versus measurement data, the method gives a significant reduction in the numbers of degrees by a factor of 1/230 in a frequency range up to 1.5 kHz. This is valid for sandwich panels of the order of 1.0–2.0 m in length compared to a modern commercial software package.
(2) The SFEM described here is also advantageous for built-up structures where the main components are uniform in length and thickness. Again this reduces the total numbers of degrees substantially if coupled to a standard finite element scheme. Inhomogeneities in geometry or material may also be treated by a standard scheme and coupled with the SFEM technique. Nevertheless, anisotropy in the core thickness may be treated by the SFEM technique if material properties vary in the vertical direction.
(3) Apart from obvious limits of applicability of the method for non-uniform regions, there is a frequency limit which depends on the cut-on frequency for cross-sectional modes. Above this limit a three-dimensional SFEM scheme is necessary.

Acknowledgements

The authors wish to thank colleagues Svante Finnveden for discussions and use of many subroutines in the spectral finite element method, Daniel Backström for use of a material parameter estimation program, and the referees for constructive comments. The authors wish to acknowledge the European Doctorate in Sound and Vibration (EDSVS) to support Paolo Bonfiglio.

Appendix. Finite element matrices

Partial integration in the x-direction, assuming $\Omega = H \times T$, the variational formulation in Section 3 leads to the system

$$\int_T \int_H (\delta\hat{\mathbf{u}}^a)^{\mathrm{T}} \left\{ \omega^2 [\mathbf{N}]^{\mathrm{T}} h[\boldsymbol{\rho}][\mathbf{N}]\hat{\mathbf{u}} - [\hat{\nabla}_z \mathbf{N}]^{\mathrm{T}}[\mathbf{C}]\hat{\nabla}_z[\mathbf{N}]\hat{\mathbf{u}} - [\hat{\nabla}_z \mathbf{N}]^{\mathrm{T}}[\mathbf{C}][\hat{\nabla}\mathbf{N}]\frac{\mathrm{d}\hat{\mathbf{u}}}{\mathrm{d}x} + [\hat{\nabla}\mathbf{N}]^{\mathrm{T}}[\mathbf{C}][\hat{\nabla}_z \mathbf{N}]\frac{\mathrm{d}\hat{\mathbf{u}}}{\mathrm{d}x} + [\hat{\nabla}\mathbf{N}]^{\mathrm{T}}[\mathbf{C}][\hat{\nabla}\mathbf{N}]\frac{\mathrm{d}^2\hat{\mathbf{u}}}{\mathrm{d}x^2} \right\} \mathrm{d}H\,\mathrm{d}x - \int_T \left[(\delta\hat{\mathbf{u}}^a)^{\mathrm{T}} [\hat{\nabla}\mathbf{N}]^{\mathrm{T}}[\mathbf{C}] \left\{ [\hat{\nabla}_z \mathbf{N}]\hat{\mathbf{u}} + [\hat{\nabla}\mathbf{N}]\frac{\mathrm{d}\hat{\mathbf{u}}}{\mathrm{d}x} \right\} \right]_H \mathrm{d}x = 0. \tag{18}$$

Matrices $[\mathbf{K}_2]$, $[\mathbf{K}_1]$, $[\mathbf{K}_0]$, and $[\mathbf{M}]$ are given by

$$[\mathbf{K}_2] = \int_H [\hat{\nabla}\mathbf{N}]^{\mathrm{T}}[\mathbf{C}][\hat{\nabla}\mathbf{N}]\,\mathrm{d}H, \tag{19}$$

$$[\mathbf{K}_1] = \int_H [\hat{\nabla}\mathbf{N}]^{\mathrm{T}}[\mathbf{C}][\hat{\nabla}_z \mathbf{N}] - [\hat{\nabla}_z \mathbf{N}]^{\mathrm{T}}[\mathbf{C}][\hat{\nabla}\mathbf{N}]\,\mathrm{d}H, \tag{20}$$

$$[\mathbf{K}_0] = \int_H [\hat{\nabla}_z \mathbf{N}]^{\mathrm{T}}[\mathbf{C}]\hat{\nabla}_z[\mathbf{N}]\,\mathrm{d}H, \tag{21}$$

$$[\mathbf{M}] = \int_H \omega^2 [\mathbf{N}]^{\mathrm{T}} h[\boldsymbol{\rho}][\mathbf{N}]\,\mathrm{d}H \tag{22}$$

and are conveniently partitioned into $m \times m$ matrices for use in setting up dynamic stiffness matrix in Section 3.1:

$$[\mathbf{K}_2] = \begin{bmatrix} \mathbf{K}^2_{uu} & \mathbf{0} \\ \mathbf{0} & \mathbf{K}^2_{ww} \end{bmatrix}, \quad [\mathbf{K}_0] = \begin{bmatrix} \mathbf{K}^0_{uu} & \mathbf{0} \\ \mathbf{0} & \mathbf{K}^0_{ww} \end{bmatrix}, \quad [\mathbf{M}] = \begin{bmatrix} \mathbf{M}_{uu} & \mathbf{0} \\ \mathbf{0} & \mathbf{M}_{ww} \end{bmatrix},$$

$$\begin{bmatrix} \mathbf{K}^1_{uu} \\ \mathbf{K}^1_{wu} \end{bmatrix} = \int_H [\hat{\nabla}\mathbf{N}]^{\mathrm{T}}[\mathbf{C}][\hat{\nabla}_z \mathbf{N}]\,\mathrm{d}H, \quad \begin{bmatrix} \mathbf{K}^1_{wu} \\ \mathbf{K}^1_{ww} \end{bmatrix} = \int_H [\hat{\nabla}\mathbf{N}]^{\mathrm{T}}[\mathbf{C}][\hat{\nabla}_z \mathbf{N}]\,\mathrm{d}H.$$

References

[1] D. Backstrom, Modelling the flexural dynamics of sandwich beams using Bernoulli–Euler or Tinoshenko theory with frequency dependent parameters, KTH, Stockholm, Sweden, TRITA-AVE 2004:45 ISSN 1651-7660, 2004.

[2] S. Sorokin, Analysis of wave propagation in sandwich plates with and without heavy fluid loading, *Journal of Sound and Vibration* 271 (2004) 1039–1062.

[3] J.S. Przemieniecki, *Theory of Matrix Structural Analysis*, McGraw-Hill, New York, 1968.

[4] F.W. Williams, W.H. Wittrick, Exact buckling and frequency calculations surveyed, *Journal of Structural Engineering* 110 (1983) 169–187.

[5] S. Finnveden, Exact spectral finite element analysis of stationary vibrations in a railway car structure, *Acta Acustica* 2 (1994) 461–482.

[6] S. Finnveden, Spectral finite element analysis of the vibration of straight fluid-filled pipes with flanges, *Journal of Sound and Vibration* 199 (1997) 125–154.

[7] A.T. Peplow, S. Finnveden, A super-spectral finite element method for sound transmission in waveguides, *Journal of the Acoustical Society of America* 116 (2004) 1389–1400.

[8] S. Dong, R. Nelson, On natural vibrations and waves in laminated orthotropic plates, *Journal of Applied Mechanics* 39 (1972) 739–745.

[9] S.B. Dong, H. Taweel, M. Kazic, Wave reflection from the free end of a cylinder with an arbitrary cross-section, *International Journal of Solids and Structures* 37 (2000) 1701–1726.

[10] P.A. Gradin, S. Widehammar, B. Lundberg, Approximate determination of dispersion relations and displacement fields associated with elastic waves in bars—method based on matrix formulation of Hamilton's principle, *Journal of Sound and Vibration* 246 (2001) 853–876.

[11] S. Datta, A. Shah, R. Bratton, T. Chakraborty, Wave propagation in laminated composite plates, *Journal of the Acoustical Society of America* 83 (6) (1988) 2020–2026.
[12] Z. Xi, G. Liu, K. Lam, H. Shang, Dispersion and characteristic surfaces of waves in laminated composite circular cylindrical shells, *Journal of the Acoustical Society of America* 108 (2000) 2179–2186.
[13] P.J. Shorter, Wave propagation and damping in linear viscoelastic laminates, *Journal of the Acoustical Society of America* 115 (2004) 1917–1925.
[14] A.T. Peplow, S. Finnveden, Calculation of vibration transmission over bedrock using a waveguide finite element model, *International Journal for Numerical and Analytical Methods for Geomechanics* (2006), submitted.
[15] B. Szabo, I. Babuska, *Finite Element Analysis*, Wiley, New York, 1991.
[16] F. Tisseur, K. Meerbergen, The quadratic eigenvalue problem, *SIAM Review* 43 (2001) 235–286.
[17] C.F. VanLoan, A symplectic method for approximating all the eigenvalues of a Hamiltonian matrix, *Linear Algebra* 61 (1984) 233–251.
[18] L. Cremer, M. Heckl, E.E. Ungar, *Structure Borne Sound*, Springer, Berlin, 1988.
[19] FEMLAB 3.1 Users Manual, Gothenburg, Sweden, 2004.